Re-**Submitted to:** *Colloid and Surface A: Physicochem. Eng. Aspects.*

Date: 20/10/2010

PIV Characterisation of Flocculation Dynamics and Floc Structure in Water Treatment

F. Xiao[a], K. M. Lam [a], X. Y. Li[a,*] , R.S. Zhong[b] and X.H. Zhang[b]

[a] Environmental Engineering Research Centre, Department of Civil Engineering, The University of Hong Kong, Pokfulam Road, Hong Kong, China

[b] Research Center for Environmental Engineering & Management, Graduate School at Shenzhen, Tsinghua University, Shenzhen, China

[*]Corresponding Author:

Phone:	(852) 2859-2659
Fax:	(852) 2559-5337
Email:	xlia@hkucc.hku.hk
Homepage:	http://web.hku.hk/~xlia/

Running Head: Particle flocculation and coagulation, Water treatment

Abstract

Particle flocculation with chemical flocculant addition is an essential step in water treatment. The performance of flocculation and the property of the flocs formed affect the overall results of the treatment process. In addition to particulate impurities, the presence of organic matter in water, such as natural organic materials (NOM), also influence the effectiveness of chemical flocculation. In this paper, the PIV system was employed to investigate the flocculation dynamics for different flocculants in different model waters. With the PIV and image analysis, the change in particle size distribution could be well recorded. Using the sequence of flocculation, shear breakage and re-flocculation on a jar-test device together with the PIV system, the rate of floc formation, the strength of the flocs, the recovery of broken flocs, and the morphological and structural features of the flocs were characterized. The results indicated that the adsorption of HA on the particle will stabilized the particles, hence hindered the flocculation process. Sweep flocculation using a higher chemical coagulant dosage was an effective means of process enhancement for the removal of particulates and associated organic matter. The dynamics of A-B-R process was characterized by particle size distribution (PSD) measurement with PIV setup. The particle strength and reversibility capability were examined. Strength index showed the HA flocs have comparable strength, while recovery index indicated a less recovery capability with the increasing of HA concentration after exposure to a higher shear, especially for ferric HA flocs. It appears that the bonds holding HA flocs together are not purely physical bonds given the limited regrowth seen. Finally, evolution of floc structure during A-B-R process was analyzed by investigated the fractal dimension D_b. The results were generally consistent with previous PSD measurements. It suggested that the structure of flocs in breakage became more compact with little permeability. An increase in floc compaction provides a further explanation for the limited regrowth for most of flocs. According to the performances of alum and ferric, it can

be noticed that HA flocs have different properties dependent on which chemical coagulant is used. Alum produced larger HA flocs which endured a higher recovery capability after exploring higher shear, hence, compared to ferric, it could be preferred to using in the practical enhanced coagulation unit.

Keywords: Aggregation-breakage-re-flocculation; humic acid; hydrodynamics; particle image velocimetry (PIV).

1. Introduction

Humic acids (HAs) are one of the main constitute of natural organic matter (NOM) in most water sources, resulting from the weathering and biodegradation of dead plants and animals [1, 2]. The presence of NOM in the water is a major concern not only to form the disinfection by-products, such as trihalomethanes (THMs), but to reduce the effectiveness of filtration processes, such as membrane fouling [3, 4]. Since United States Environmental Protection Agency has proposed that enhanced coagulation is a best available technology for NOM removal [5, 6], extensive studies are addressed on the performance of humic acid coagulation [7-9], however little thought is given to the physiochemical characteristics of HA flocs. It includes floc size, compaction, strength and the potential to regrow after being broken.

Enhanced coagulation is still a shear-induced flocculation, which means the shear flow is a main reason to result in collisions which cause the flocs to grow. However, they can still be subjected to higher shear rates where the flocs have to resist the corresponding stresses [10]. By use of model spherical particles, such as latex beads, it has been previously shown that particle suspensions destabilized with an ionic salt (i.e. NaCl) will reform to their initial size if the original velocity gradient is subsequently reapplied [11]. This behaviour is known as reversible breakage. However, in most instances where conventional metal coagulants and polymers are used for the aggregation of small particle suspensions (such as precipitated solids), irreversible breakage is usually seen, such that the initial floc size is never subsequently achieved after breakage.

The irreversibility of aggregates during cycled shear is most likely the result of particle-flocculant bond breakage during fragmentation, hence the reorganisation and restructuring can both occur. Experimental shear-induced coagulation-fragmentation processes [11-14] found that the fractal dimension shifts to a larger value compared to the

initial one, which showed a more compact structure formed during the cycled shear. However, there has been no previous work showing the regrowth potential of HA flocs with different coagulants and the structure restructuring and reorganisation during a cycled shear schedule. Thus, an understanding of the reversible potential for natural organic flocs may provide an important addition to the well-studied field of HA enhanced flocculation.

The structure of the HA containing flocs is non-homogeneous and should be described by the fractal scaling law [15-17]. This fractal structure would affect the properties of the flocs during aggregation-breakage-regrowth process. Although, more research effort has been made to specify the properties of HA containing flocs, there is no study to report the exact influence of the fractal structure on the hydrodynamic behaviours of flocs formed in water treatment. Therefore, it merits more efforts to investigate the hydrodynamic properties of the HA containing flocs and their relationship with the fractal structure of the flocs.

In present work, a series of the standard jar-tests were carried out to predict the overall result of water flocculation and sedimentation. ζ-potential, turbidity removal and HA reduction were determined for the particle suspension at various coagulant dosage. An improved experimental facility for characterization of the PSD dynamics was developed by making use of particle image velocimetry (PIV) coupled with image-analysis system. This non-intrusive measurement of PSD was performed to characterize the HA flocs during aggregation-breakage-regrowth (A-B-R) process. Morphology evolution indicated by surface fractal dimension, breakage and regrowth potential of different HA flocs were evaluated with different coagulants.

2. Materials and Methods

2.1 Model waters and jar-test flocculation experiments

Humic acid (HA) (Florida peat humic acid reference: 1R103H-2) was obtained from International Humic Substances Society, and the stock HA solution was made by dissolving the HA into de-ionized water. Kaolin (Aldrich, Milwaukee, WI) with a mean size of around 2.6 μm was used for making particle suspensions. Three types of the model waters that contained 10 mg/L kaolin with an initial turbidity of 12 NTU and different HA contents were prepared for the experimental study, including (1) HA0 – no HA addition, (2) HA3 - 3 mg/L HA in water measured in terms of dissolved organic carbon (DOC), and (3) HA10 - 10 mg DOC/L of HA. Two flocculants – alum ($Al_2(SO_4)_3 \cdot 14H_2O$) (BDH Chemicals, England) and ferric chloride ($FeCl_3 \cdot 6H_2O$) (UNI-Chem, Mumbai, India) - were tested for the flocculation performance.

Standard jar-test flocculation and sedimentation experiments were conducted at room temperature (~22 °C) on the model waters with a jar-test device (ZR4-6, Zhongrun, Shenzhen, China). The jar-tester consisted of six 1-L rectangular beakers, each was filled with 500 mL water, and the mixing was provided by with flat paddle mixers (5.0 × 4.0 cm^2). For each model water, a flocculant, alum or ferric, was added at various dosages from 0 to 50 mg/L into the six beakers. Throughout a flocculation experiment, the water pH was monitored by a pH meter (420A, Orion, Boston, MA). 1 M $NaHCO_3$ was used to adjust the solution pH to a proper range for the different flocculant dosages, i.e. pH~7.0 for alum flocculation and pH~6.5 for ferric flocculation.

For a jar-test run, the water after the chemical addition was mixed rapidly at 100 rpm for 60 sec. A sample of 10 mL was then withdrawn from each beaker for particle ζ-potential measurement by a laser ζ-potential analyzer (Delsa 440SX, Coulter, Amherst, MA). Following the rapid mixing, the water in the jar-test beakers was mixed for flocculation at a slower rate of 30 rpm for 40 min followed by 30 min of sedimentation. The supernatant was collected, for which the turbidity and HA residues were analyzed. The turbidity was

measured with a Turbidimeter (2100N, HACH, Loveland, CO), and the DOC in water was measured by a TOC analyzer (5000A, Shimadzu, Kyoto, Japan). In addition, based on the ζ-potential measurement and jar-test results, the optimal dose of a flocculant for a model water could be determined. The optimal dose was then used for the flocculation-breakage-reflocculation experiment on the model water characterized by the PIV technique.

2.2 Particle image velocimetry (PIV) for particle size distribution measurement

A PIV system was employed to track the change in particle size distribution (PSD) during a flocculation experiment. PIV is an advanced and powerful flow visualization and particle tracking technique [18]. As a non-intrusive optical setup, the PIV was able to capture the image of particles in a jar-test beaker within a millisecond (Figure 1). The PIV system consists of a laser illumination setup, a high-speed CCD video camera and a process control and image processing software package. A pulsed laser beam generated from the source (Coherent, Inc., Santa Clara, USA) was expanded to a thin laser light sheet by a combination of a cylindrical and a spherical lenses. The laser sheet illuminated a planar region of the water for visualization of the particles and flocs in the flocculation tank (beaker). The images of laser-illuminated particles could be captured by a high speed CCD camera (PCO.imaging 1200 with a resolution of 1280×1024 pixels). The PIV system was controlled by a computer with dedicated software (PCO.camware) for laser flushing, CCD recording, image acquisition and storage. Images were processed with an image analysis system (Scion Image, Frederick, MD) for PSD determination. For a floc of irregular shape, its size, d, was calculated in terms of the equivalent diameter by $d = (4A/\pi)^{1/2}$, where A is the projected area of the floc. Based on calibration, the PIV system had a resolution of around 9 μm for particle tracking and imaging in the present flocculation study. More than 40 consecutive images within a minute were

analyzed to produce a size distribution of the particles, and the result was presented as either a number-based discrete PSD or a volume-based discrete PSD.

In addition to size measurement, particle image analysis also can provide more information about the morphological and structural feature of the aggregate flocs. For the 2-D projected particle images, a boundary fractal dimension was used to characterize the fractal property of the flocs. The boundary fractal dimension defines how the projected areas of the particles scale up with the length of the perimeter [14, 16]. Accordingly, the boundary fractal dimension, D_b, may be determined from the correlation [16, 19] as follows,

$$A \propto P^{2/D_b} \tag{3}$$

where P is the perimeter of an aggregate. D_b ranges from 1 to 2, and there is no straightforward relationship between D_b and the mass fractal dimension for a particle population [15]. Nonetheless, a higher D_b value often suggests a more fractal structure of the objects with a less spherical shape and irregular or rough surface [16].

2.3 Flocculation-breakage and reflocculation test for floc strength and re-growth

A single beaker jar-test device was used together with the PIV for characterization of the flocculation dynamics (Figure 1). The jar-tester included a glass rectangular tank (L×W×H = 80 × 80 × 200 mm) equipped with a flat paddle mixer that was driven by a DC power supply. The flocculation procedure on a model water was the same as previous described, i.e., after the chemical addition a pre-determined dose, the water was stirred rapidly at 100 rpm for 60 s followed by a slow mixing at 30 rpm for 30 min. Upon the completion of flocculation, the shear breakage and then re-flocculation experiment was carried out. The breakage of flocs was conduced at 100 rpm for 15 min, which was followed by re-flocculation with slow mixing at 30 rpm for 30 min. During the course of flocculation-

157 breakage-reflocculation, the images of particles and flocs in water was recorded and analyzed
158 by the PIV system. The PSDs at different phases of the process were therefore obtained.
159 The inter-particle bonds that hold aggregate flocs together are considered as the
160 cohesive strength of the flocs. A size ratio method [20] is used here with an index (σ) to
161 express the strength of particle flocs, i.e.,

162 $$\sigma = d_2 / d_1 \quad (1)$$

163 where d_1 and d_2 are the mean sizes of the flocs before and after the shear breakage,
164 respectively. A higher value of the σ index indicates a higher strength of the flocs to resist
165 breakage when exposed to an elevated fluid shear.
166 When the shear intensity was reduced after the breakage phase, re-flocculation of the
167 particles could take place. A reversibility factor is used here to measure the re-flocculation
168 potential of the particles when the shear is reinstalled to its original level. A modified size
169 ratio approach may be applied to calculate the reversibility (γ) by

170 $$\gamma = \frac{d_3 - d_2}{d_1 - d_2} \quad (2)$$

171 where d_3 is the mean size of the particle flocs after re-flocculation at the original shear rate. A
172 higher reversibility index suggests a greater flocculation and re-growth capability of the flocs
173 after the shear breakage.
174
175 **3. Results and Discussion**
176
177 *3.1 Coagulation performance and water treatment results*
178 *3.1.1 ξ-potentials of the kaolin particles at different flocculant doses*
179 The clean kaolin was negatively charged with an average ζ-potential of around -30
180 mV (Figure 2). The presence of HA apparently increased the intensity of negative charges on

the particles, and the ζ-potential became more negative to -46 mV or below. Hence, HA would cause further stabilization of particles in water. This is likely due to the steric or elastic repulsion between particles brought about by the humic substances [21-23]. As anticipated, addition of the flocculants, alum or ferric, could effectively reduce the surface charge of the particles in all types of the model waters, resulting in particle destabilization. As the flocculant dose increased, the particle ζ-potentials in the model waters approached zero. Further increase in flocculant dose caused a certain extent of charge reversal of the particles (Figure 2).

For pure kaolin with no HA in water, a small amount of the flocculants (5 mg/L or lower) would eliminate the ζ-potentials and destabilize the particles completely. As the HA content increased, the amount of alum or ferric required to achieve the same level of ζ-potential reduction increased considerably. In comparison, alum appeared to be more effective than ferric for reducing the ζ-potential of kaolin particles (Figure 2). For example, with alum flocculation, the dose to neutralize the surface charge of kaolin was about 20 mg/L for the HA3 water and 30 mg/L for the HA10 water. In ferric chloride flocculation, the corresponding dose for charge neutralization was around 25 mg/L for HA3 and 30 mg/L for HA10.

3.1.2 Jar-test results of the flocculation and turbidity removal

The jar-test flocculation and sedimentation results for turbidity and HA removals from the model waters were in general agreement with would be expected from the ζ-potential analysis. For clean kaolin without HA, a low flocculant dose of 5 mg/L was sufficient to bring about flocculation for turbidity removal (Figure 3). With the presence of HA in water, the flocculant demand for particle flocculation and turbidity removal increased significantly. Alum appeared to be slightly more effective than ferric chloride for particle

206 flocculation. Nonetheless, a low alum dose below 20 mg/L still left a high level of HA
207 residue in water after flocculation and sedimentation. For the HA10 water with a high HA
208 content, at least 20 mg/L of alum or 25 mg/L of ferric chloride was needed to have
209 satisfactory flocculation and turbidity removal.

210 Enhanced flocculation with a high flocculant dose was effective to remove humic
211 substances from water (Figure 3). However, further increase of alum beyond 40 mg/L did not
212 bring about a notable improvement in turbidity and HA removals. For ferric chloride
213 flocculation, a dose of more than 40 mg/L actually worsened kaolin flocculation, particularly
214 for the HA0 and HA3 waters, resulting in poor turbidity removal. Judging from the ζ-
215 potential changes and jar-test results, the optimal alum doses chosen for the PIV-flocculation
216 experiments on the HA0, HA3 and HA10 waters were 10, 20 and 30 mg/L at pH~7.0,
217 respectively, and the optimal ferric chloride doses were 10, 25, and 30 mg/L at pH~6.5,
218 respectively.

219

220 *3.2 PSD dynamics, floc strength and re-flocculation capability*

221 *3.2.1 PIV characterisation of the flocculation dynamics*

222 The PIV technique is shown to be a powerful tool for obtaining the particle size
223 distributions in a dynamic fluid system. The PIV is a true non-intrusive particle tracking
224 system that is able to perform real-time *in-situ* particle imaging acquisition for determination
225 of the PSD dynamics during shear flocculation. The PSD of the flocs was expressed as the
226 volume-based discrete PSD, i.e. the percentages of the total particle volume observed against
227 a series of size sections (Figure 4).

228 The PIV results showed the continuous floc formation and growth in the model waters
229 during the chemical flocculation process. The PSD maintained a constant unimodal shape
230 with an apparent peak. Accordingly, the peak size, the particle size section corresponding to

231 the peak of the PSD curve, was used here as the mean size of the particle population observed
232 by the PIV. The change in the peak size of PSD with time illustrated well the flocculation-
233 breakage dynamics for a particle system. For both alum and ferric flocculation at the
234 respective optimal doses, flocs were well formed with a peak size of 1000 μm or larger. The
235 PSDs became rather stable in shape and position by the end of 30 min slow flocculation at 30
236 rpm. Shear breakage at a high stirring rate (100 rpm) caused a rapid and remarkable shift of
237 the PSDs to smaller sizes, and re-flocculation took place when the fluid shear was reduced
238 (Figure 4).

239 The PSD evolution showed effective alum and ferric flocculation on the jar-test
240 device (Figure 4). For either one of the flocculants, the HA0 water with pure kaolin and no
241 HA had the largest flocs formed, followed by the HA3 water and then the HA10 water. The
242 humic substances in water reduced the effectiveness of the flocculants in forming larger flocs.
243 However, with the higher doses used for HA3 and HA10 than that for HA0, floc formation in
244 the HA3 and HA10 waters occurred at a faster rate in the early phase of flocculation than that
245 in the HA0 water. In comparison, flocculation by alum produced larger flocs than ferric
246 chloride for the same water samples (Table 1). Nonetheless, compared to alum, ferric
247 chloride flocculation took place more rapidly after the chemical addition. For both
248 flocculants, the growth of particle flocs became much slower approaching the end of 30 min
249 slow flocculation.

250

251 *3.2.2 Breakage of the flocs and their re-flocculation*

252 A sudden increase in shear rate in the jar-test led to dramatic breakage of the
253 aggregate flocs in all water samples. Within 1 min or so, the peak sizes of the PSDs were
254 more than halved, according to the PIV observations (Figure 5). In agreement with previous
255 findings [19, 24], the large alum or ferric flocs formed by slow flocculation were rather

fragile and vulnerable to shear breakage. After the initial break-up, the breakage of the flocs became much slower in the later phase of the breakage step. Thus, as suggested by others [25-27], a shear breakage process may be classified into two phases. In the first phase, rapid fragmentation of the flocs was the dominant phenomenon. In the following phase, particle erosion could be the main cause for the slower decrease of floc sizes. Between the two flocculants, ferric flocs appeared to be broken more easily to smaller flocs than alum flocs (Figure 5).

As the shear was reduced to the original level, re-flocculation of the particles took place, but to different extents in different model waters. Alum flocs were seen to have considerable re-growth in size by flocculation (Figure 5). In comparison, ferric flocs were more difficult to be recovered after breakage. The HA0 water showed the highest level of re-flocculation for both flocculants, followed by HA3 and HA10. The humic matter in flocs apparently decreased their potential of aggregation. In general, re-flocculation of the broken particle flocs was a much slower process than the original flocculation after the flocculant addition. Meanwhile, except for the alum flocs in HA0, the flocs recovered by re-flocculation were much smaller in size than the flocs before breakage.

3.2.3 Strength and recoverability of the alum and ferric flocs

Based on the change in peak size of the PSD, the strength and reversibility of the particle flocs formed in different model waters were determined (Table 1). After 15 min of shear breakage, the alum flocs in HA0 showed the highest strength index at 32%. Other types of flocs, including the alum flocs in HA3 and HA10 and all of ferric flocs had the strength indexes that were rather similar to each other. In re-flocculation at a slower shear rate, the alum flocs after breakage generally had a higher potential of recovery than the ferric flocs. Pure kaolin flocs formed by alum flocculation had a of recovery index of 46%. As the HA

content in water increased, the recovery indexes of the broken flocs decreased significantly. The alum flocs in HA10 had a low reversibility of only 10%. In agreement with the PIV observations, the ferric flocs in HA10 after breakage almost could not be re-flocculated with a recovery index as low as 4%.

3.3 Morphology and Fractal Dimension of the Flocs

3.3.1 Morphology and boundary fractal dimension of the flocs

The high-quality PIV images (Figure 6) also allow detailed analysis of the morphology and structural features of the flocs suspended in water. According to equation 3, the boundary fractal dimension of the particle flocs can be approximated from the slope of the log-log regression of a series of projected areas versus perimeters of the particles. The D_b of the flocs ranged from 1.11 to 1.22 after 30 min of slow flocculation (Figure 7). This is somewhat lower than the value of from 1.1 to 1.4 reported for the aggregates of polystyrene spheres [19]. For alum flocculation, flocs in the HA3 and HA10 waters had a slightly higher D_b than that in HA0. For ferric chloride flocculation, flocs in HA10 had the highest D_b, followed by HA3 and then HA0.

A higher D_b normally indicates a more irregular and/or elongated shape and a rougher surface for the particles, whilst a lower D_b suggests a more spherical shape and a smoother surface of the particles. Based on the D_b values, the flocs formed in the HA0 water at a low alum or ferric chloride dose were less fractal with a more regular shape and smooth surface. In comparison, the alum and ferric flocs formed by enhanced flocculation at higher flocculant doses were more fractal with an elongated shape and a rougher surface.

3.3.2 Change of the floc morphology during breakage and re-flocculation

After the shear breakage, flocs in all of the model waters were smaller and became less fractal in shape with reduced D_b values (Figure 7). When exposed to a higher shear, it is expected that the flocs would break at their weak points and rearrange into more stable structures [11, 28]. Fragmentation of the elongated flocs would break up the flocs into smaller pieces that were more close to spherical objects than the original flocs. As described previously, re-flocculation at a reduced shear rate resulted in regrowth of the floc sizes. Meanwhile, the fractal structure of the particle flocs was recovered partially as indicated by an increase in fractal dimension. Nonetheless, similar to the PSDs, the D_b of the flocs could not be fully recovered to their original levels (Figure 7). After re-flocculation, the D_b values of the alum flocs generally were somewhat higher than those of the ferric flocs, which was in agreement with the indication of the recovery index of the broken flocs (Table 1).

3.3.3 Effect of the humic content on particle flocculation and floc strength.

The addition of chemical coagulants would impose mainly two aspects of impact on particle flocculation in water. One effect is to destabilize particles in a suspension, which enhances particle flocculation. The other effect is to form hydrolyzing metal salts and their precipitates that adsorb particle colloids. [23, 29] pointed out that flocs formed following charge neutralization should have a high recoverability after breakage. In comparison, the precipitates of hydrolyzed flocculants would have a much lower recoverability after breakage [24, 30]. In the HA0 water with pure kaolin and no HA, the low dose of the coagulants could destabilize kaolin in the suspension by charge neutralization prior to particle flocculation. Nonetheless, the partially reversible breakage of the HA0 flocs suggests that the formation of the hydrolyzed flocculant precipitates and the adsorption of kaolin by the flocs of the precipitates also played an important role in removing particulate turbidity from water. For the HA3 and HA10 waters, more flocculants had to be used for kaolin adsorption and

removal. At a high flocculant dose, larger flocs of the precipitates would be formed more easily. In agreement with previous findings [24, 30], these types of the flocs of hydrolyzed precipitates in HA3 and HA10 waters had a lower recoverability after breakage compared to the HA0 flocs (Table 1).

The content of organic matter appeared to be an important factor to determine the surface properties of formed flocs, such as adhesion, inter-particle interaction and floc stability [9, 31-32]. The HA content also affects the surface fractal dimension of the particle flocs [33]. In this study, the HA presence apparently facilitated the formation of a more porous and more fractal structure corresponding with a higher D_b (Figure 7). These results are well consistent with the findings of [33]. They found that untreated kaolin formed flocs with a less fractal and more regular structure and the flos of kaolin with HA attained a more irregular and more fractal structure.

4. Conclusion

A series of standard jar-test flocculation experiments were performed on the model waters with kaolin and various amounts of humic acids, 0 (HA0), 3 mg/L (HA3) and 10 mg/L (HA10). Judging from the ζ-potential changes and the jar-test results, the optimal alum doses for the HA0, HA3 and HA10 waters were 10, 20 and 30 mg/L, respectively, and the optimal ferric chloride doses were 10, 25, and 30 mg/L, respectively.

The PIV technique was employed successfully to record and characterize the PSD dynamics during the flocculation process in water treatment. The PIV system together with the image analysis technique is capable to track the change in PSD on a jar-test during particle flocculation and floc breakage and re-flocculation. Based on the change in the peak size of the PSD, the strength and reversibility of the particle flocs formed in different model waters were determined. The results showed that the alum flocs were somewhat stronger than

the ferric flocs. As the HA content in water increased, the recovery index of the flocs after breakage decreased significantly. The alum flocs in HA10 had a reversibility of only 10%, while the ferric flocs in HA10 after breakage could hardly be re-flocculated with a recovery index as low as 4%.

According to the PIV images, the flocs formed initially after the flocculant addition were larger and more fractal with a higher value of boundary fractal dimension D_b. After shear breakage, the flocs became smaller and less fractal with a lower D_b. With the re-flocculation, the fractal structure of the flocs could be only partially recovered. The results suggested that initially aggregates have a ramified, open structure that became more compact as exposure to a higher shear. An increase in floc compaction would lead to a reduction in floc size, which provides a further explanation for the limited regrowth of most flocs. The broken flocs seemed to become somehow difficult to form previous porous and fractal clusters. It indicated the chemical bonds or/and chemical adsorption formed in first aggregation phase were broken and flocs become more stable and rearrange into more compact structure during the recovery stage.

Acknowledgements

This research was supported by grants HKU7149/E06 and HKU7144/E07 from the Research Grants Council (RGC) and the funding of AoE/P-04/2004 from the University Grants Council (UGC) of the Hong Kong SAR Government. The technical assistances of Mr. Keith C. H. Wong and Mr. C. H. Tong are greatly appreciated.

References

[1] S. Chang, R.A. Berner, Humic substance formation via the oxidative weathering of coal. Environ. Sci. Technol. 32 (1998) 2883-2886.

[2] W.P. Cheng, F.H. Chi, A study of coagulation mechanisms of polyferric sulfate reacting with humic acid using a fluorescence-quenching method. Water Res. 36 (2002) 4583-4591.

[3] A. Thekkedath, W.M. Naceur, K. Kecili, M. Sbai, A. Elana, L. Auret, H. Suty, C. Machinal, M. Pontie, Macroscopic and microscopic characterizations of a cellulosic ultrafiltration (UF) membrane fouled by a humic acid cake deposit: First step for intensification of reverse osmosis (RO) pre-treatments. C. R. Chimie 10 (2007) 803-812.

[4] A. Rubia, M. Rodriguez, V.M. Leon, D. Prats, Removal of natural organic matter and THM formation potential by ultra- and nanofiltration of surface water. Water Res. 42 (2008) 714-722.

[5] EPA, Enhanced coagulation and enhanced precipitative softening guidance manual. EPA 815-R-99-012, 1999.

[6] J.K. Edzwald, Enhanced coagulation: US requirements and a broader view. Water Sci. Technol. 40 (1999) 63-70.

[7] D. Schmitt, H.E. Taylor, G.R. Aiken, D.A. Roth, F.H. Frimmel, Influence of natural organic matter on the adsorption of metal ions onto clay minerals. Environ. Sci. Technol. 36 (2002) 2932-2938.

[8] Y. Wang, B. Du, J. Liu, B. Shi, H. Tang, Surface analysis of cryofixation-vacuum-freeze-dried polyaluminum chloride–humic acid (PACl–HA) flocs. J. Colloid Interface Sci. 316 (2007) 457-466.

[9] X. Y. Li, U. Passow, B. E. Logan, Fractal dimension of small (15-200 μm) particles in Eastern Pacific coastal waters. Deep-Sea Res. 45 (1998) 115-118.

[10] N.D. Vassileva, van den D. Ende, F. Mugele, J. Mellema, Fragmentation and erosion of two-dimensional aggregates in shear flow. Langmuir 23 (2007) 2352-2361.

[11] P.T. Spicer, S.E. Pratsinis, J. Raper, R. Amal, G. Bushell, G. Messters, The reversibility of floc breakage. Powder Technol. 97 (1998) 26-34.

[12] V. Oles, Shear-induced aggregation and breakage of polystyrene latex particles. J. Colloid Interf. Sci. 154 (1992) 351-358.

[13] K. A. Kusters, S. E. Pratsinis, S. G. Thoma, D. M. Smith, Ultrasonic fragmentation of agglomerate powders. Chem. Eng. Sci. 48 (1993) 4119-4127.

[14] T. Serra, X. Casamitjana, Structure of the aggregates during the process of aggregation and breakup under a sheer flow. J. Colloid Interface Sci. 206 (1998) 505-511.

[15] P. Meakin, Fractal aggreages. Adv Colloid Interface Sci. 28 (1988) 249-331.

[16] Q. Jiang, B.E. Logan, Fractal dimensions of aggregates determined from steady-state size distributions. Environ. Sci. Technol. 25 (1991) 2031-2038.

[17] S.R. Grey, C.B. Ritchie, T. Tran, B.A. Bolto, Effect of NOM characteristics and membrane type on microfiltration performance. Water Res. 41 (2007) 3833-3841.

[18] M. Raffel, C.E. Willert, J. Kompenhans, Particle image velocimetry: a practical guide. Springer, Berlin, 1998

[19] P.T. Spicer, S.E. Pratsinis, Coagulation and fragmentation: Universal steady-state particle-size distribution. AIChE J. 42 (1996) 1612-1620.

[20] P. Jarvis, B. Jefferson, J. Gregory, S.A. Parsons, A review of floc strength and breakage. Water Res. 39 (2005) 3121-3137.

[21] M. Elimelech, J. Gregory, X. Jia, R. A. Williams, Particle deposition and aggregation: measurement, modelling and simulation, Butterworth-Heinemann, Woburn, MA, 1995. p9–63, 261–289.

[22] M. Stumm, J.J. Morgan, Aquatic Chemistry: Chemical Equilibrium and Rates in Natural Waters. Wiley, New York, 1995.

[23] A. Amirtharajah, C.R. O'Melia, Coagulation processes: Destabilisation, Mixing and Flocculation. In AWWA Water Quality and Treatment: a Handbook of Community Suppliers. McGraw-Hill, New York, 1999.

[24] R.J. Francois, Ageing of aluminum hydroxide flocs. Water Res. 21 (1987) 523-531

[25] D.S. Parker, W.J. Kaufman, D. Jenkins, Floc breakup in turbulent flocculation processes. Journal of the Sanitary Engineering Division-ASCE 98 (NSA1) (1976) 79-99.

[26] P.A. Shamlou, S. Stavrinides, N. Titchener-hooker M. Hoare, Growth-independent breakage frequency of protein precipitates in turbulently agitated bioreactors. Chem. Eng. Sci. 49 (1994) 2647-2656.

[27] C.A. Biggs, P.A. Lant, Activated sludge flocculation: On-line determination of floc size and the effect of shear. Water Res. 34 (2000) 2542-2550.

[28] C. Selomulya, R. Amal, G. Bushell, T.D. Waite, Evidence of shear rate dependence on restructuring and break-up of latex aggregates. J. Colloid Interface Sci. 236 (2001) 67-77.

[29] V. Chaignon, B.S. Lartiges, A.El. Samrani, C. Mustin, Evolution of size distribution and transfer of mineral particles between flocs in activated sludges: an insight into floc exchange dynamics. Water Res. 36 (2002) 676-684.

[30] K. McCurdy, K. Carlson, D. Gregory, Floc morphology and cyclic shearing recovery: comparison of alum and polyaluminum chloride coagulants. Water Res. 38 (2004) 486-494.

[31] M.R. Jekel, The stabilization of dispersed mineral particles by adsorption of humic substances. Water. Res. 20 (1996) 1543 – 1554.

[32] B. Janczuk, T. Białopiotrowicz, A. Zdziennicka, M. Hajnos, G. Jozefaciuk, The influence of soil clay constituents on surface free energy of clay fractions. J. Soil Sci. 43 (1992) 27–35.

[33] Z. Sokolowska, S. Sokolowski, Influence of humic acid on surface fractal dimension of kaolin: analysis of mercury porosimetry and water vapour adsoption data. Geodema 88 (1998) 233-249.

Figure captions

Figure 1. Schematic diagram of the PIV coupling with an image analysis system.

Figure 2. ζ-potential of the three particle systems as a function of the coagulant dose.

Figure 3. Turbidity and TOC after the jar-test flocculation and sedimentation experiments as a function of the flocculant dose for the three particle systems.

Figure 4. PSD profiles of the particles flocs for different HA contents in water during the A-B-R process.

Figure 5. Change of the peak size of flocs for different HA contents in water during the A-B-R tests.

Figure 6. Examples of the PIV images of particle flocs during a typical A-B-R process.

Figure 7. Change of the fractal dimension of the particle flocs with different HA contents in water during the A-B-R tests.

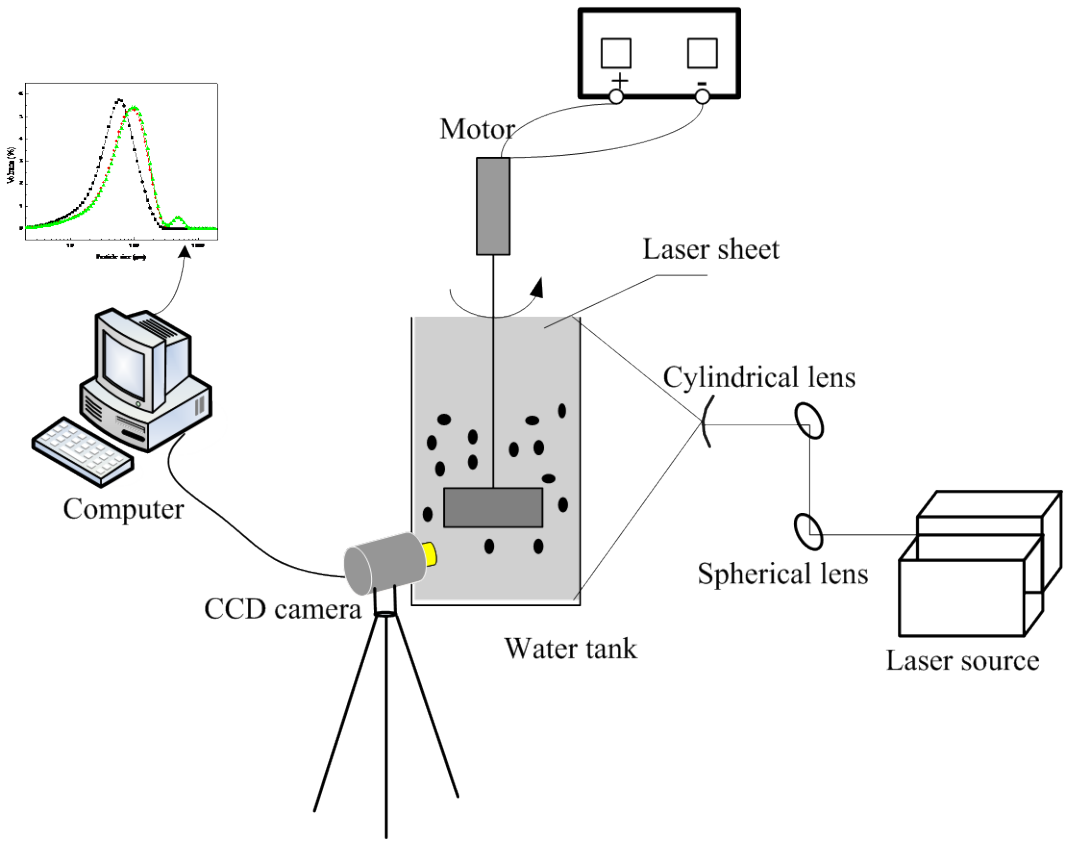

Figure 1. Schematic diagram of the PIV coupling with an image analysis system.

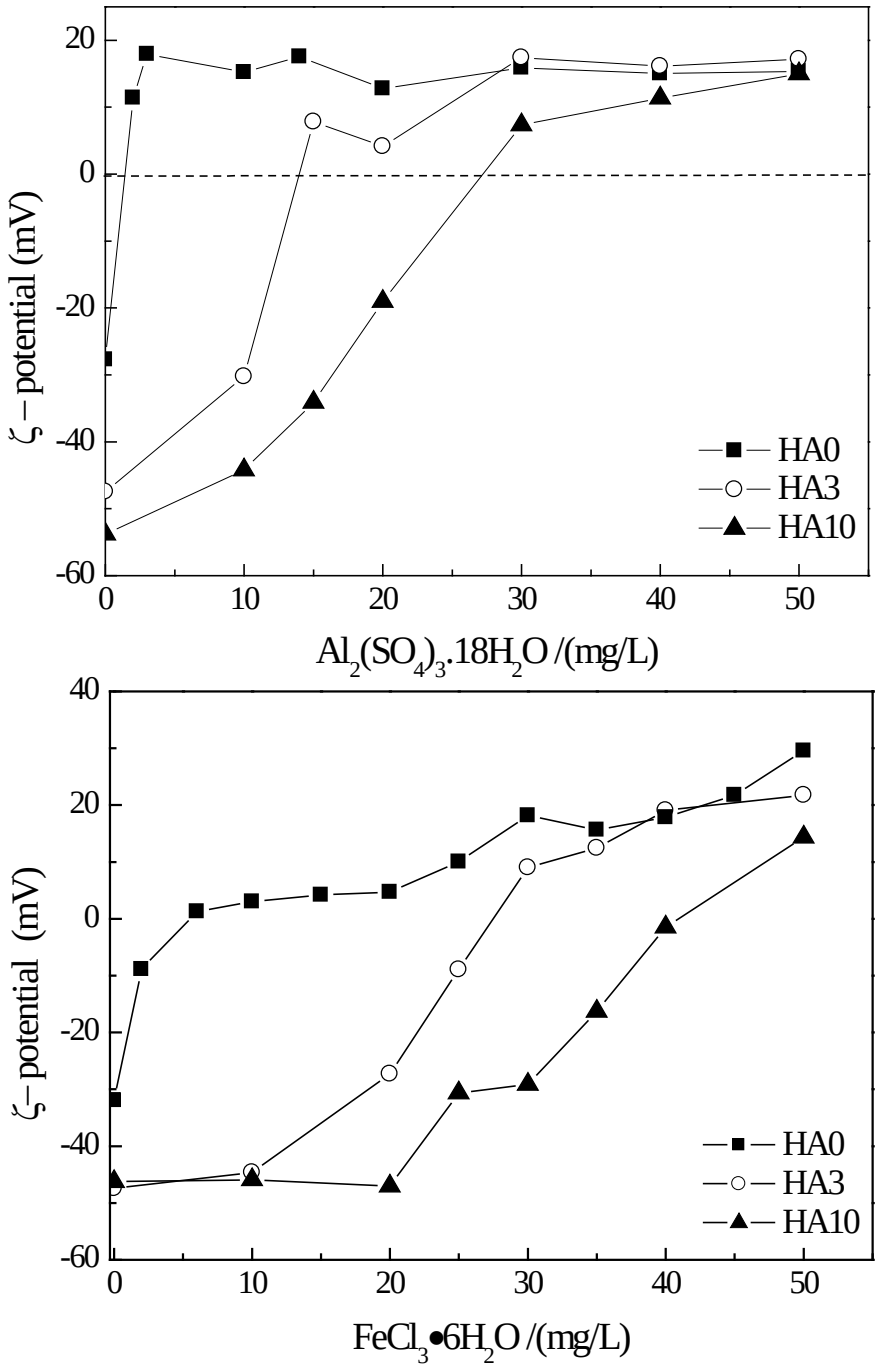

477

478 **Figure 2.** ζ-potential of the three particle systems as a function of the coagulant dose.

479

480

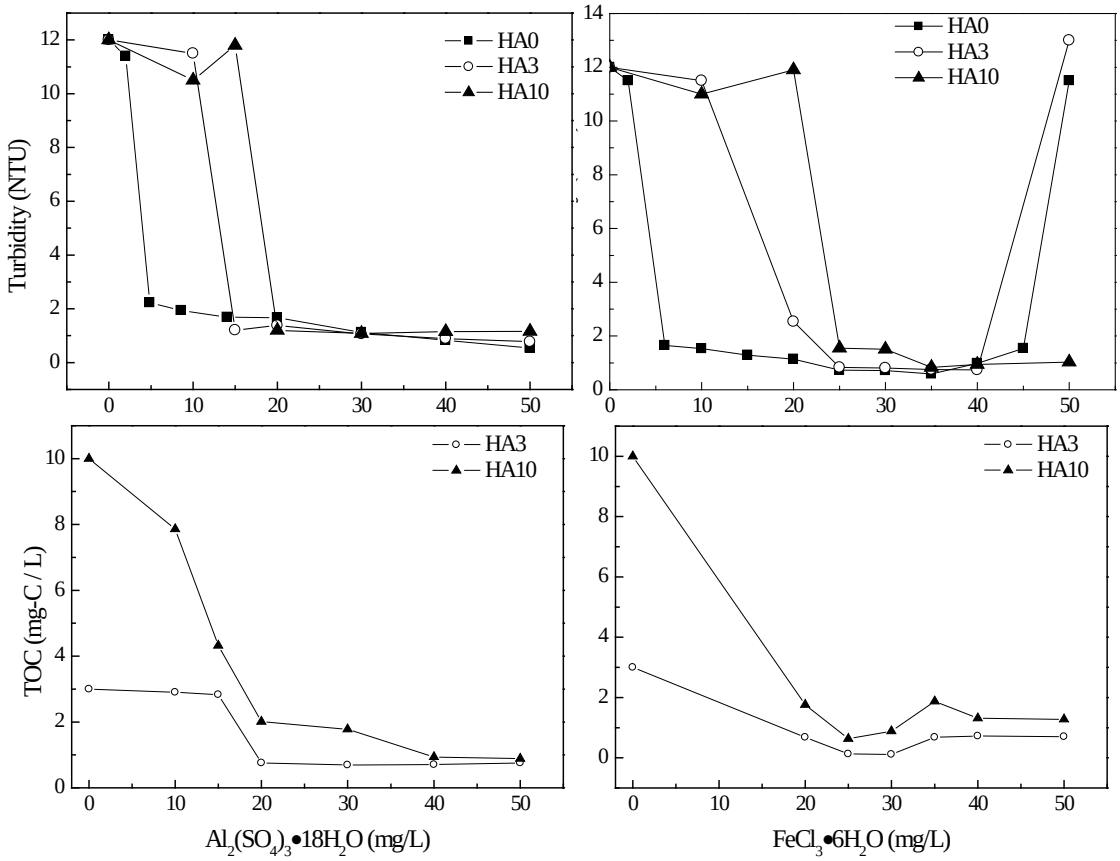

Figure 3. Turbidity and TOC after the jar-test flocculation and sedimentation experiments as a function of the flocculant dose for the three particle systems.

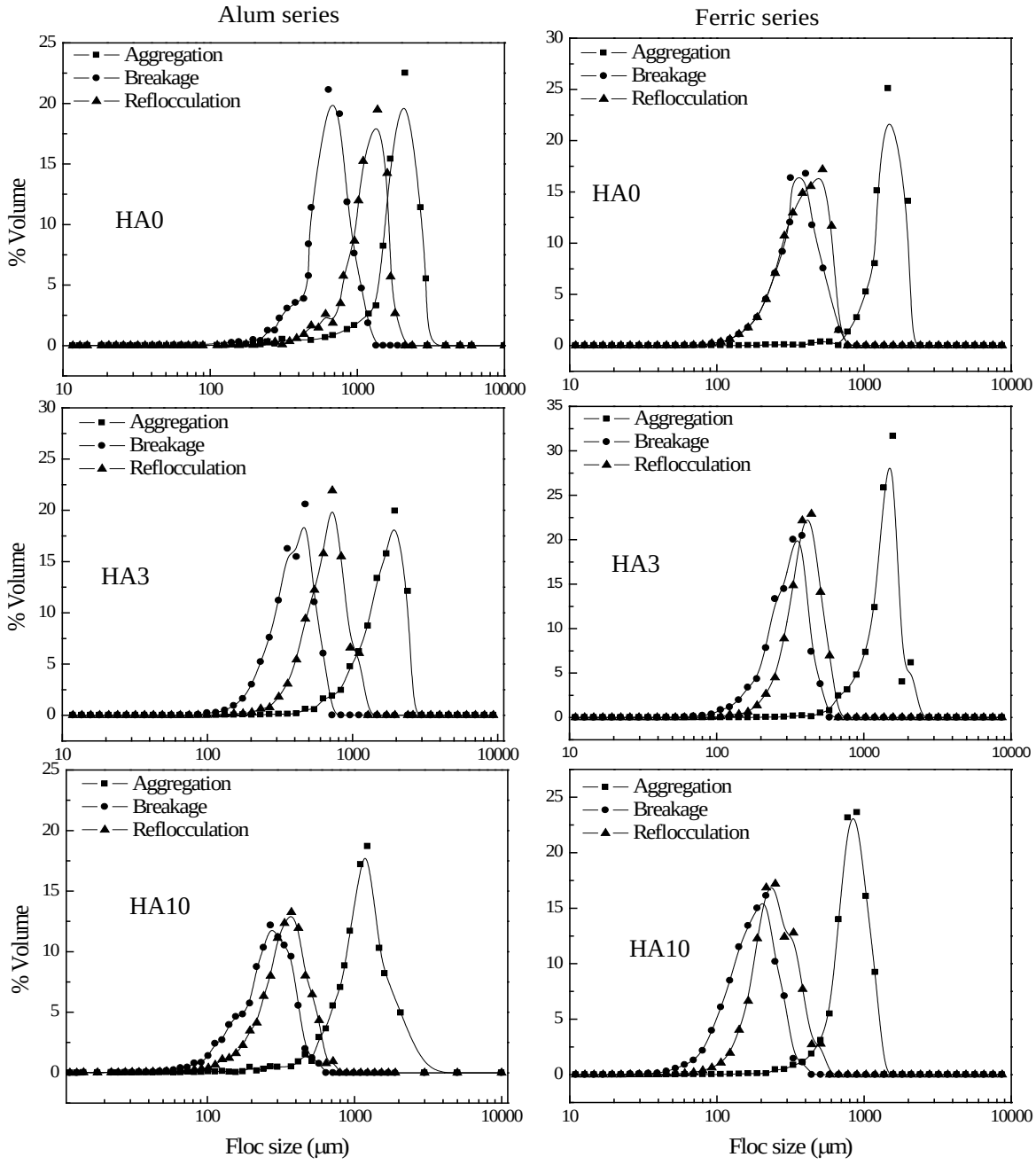

Figure 4. PSD profiles of the particles flocs for different HA contents in water during the A-B-R process.

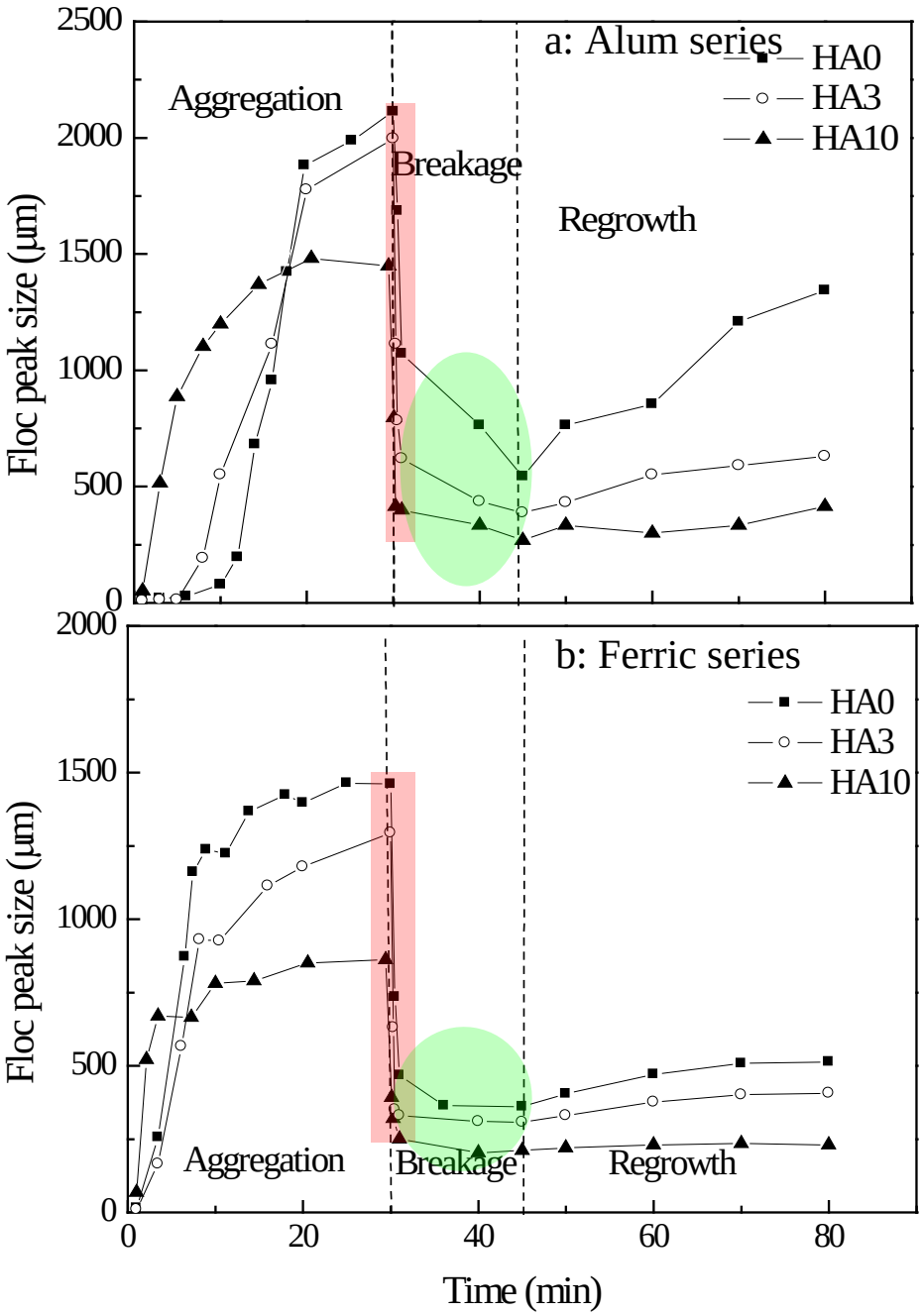

Figure 5. Change of the peak size of flocs for different HA contents in water during the A-B-R tests.

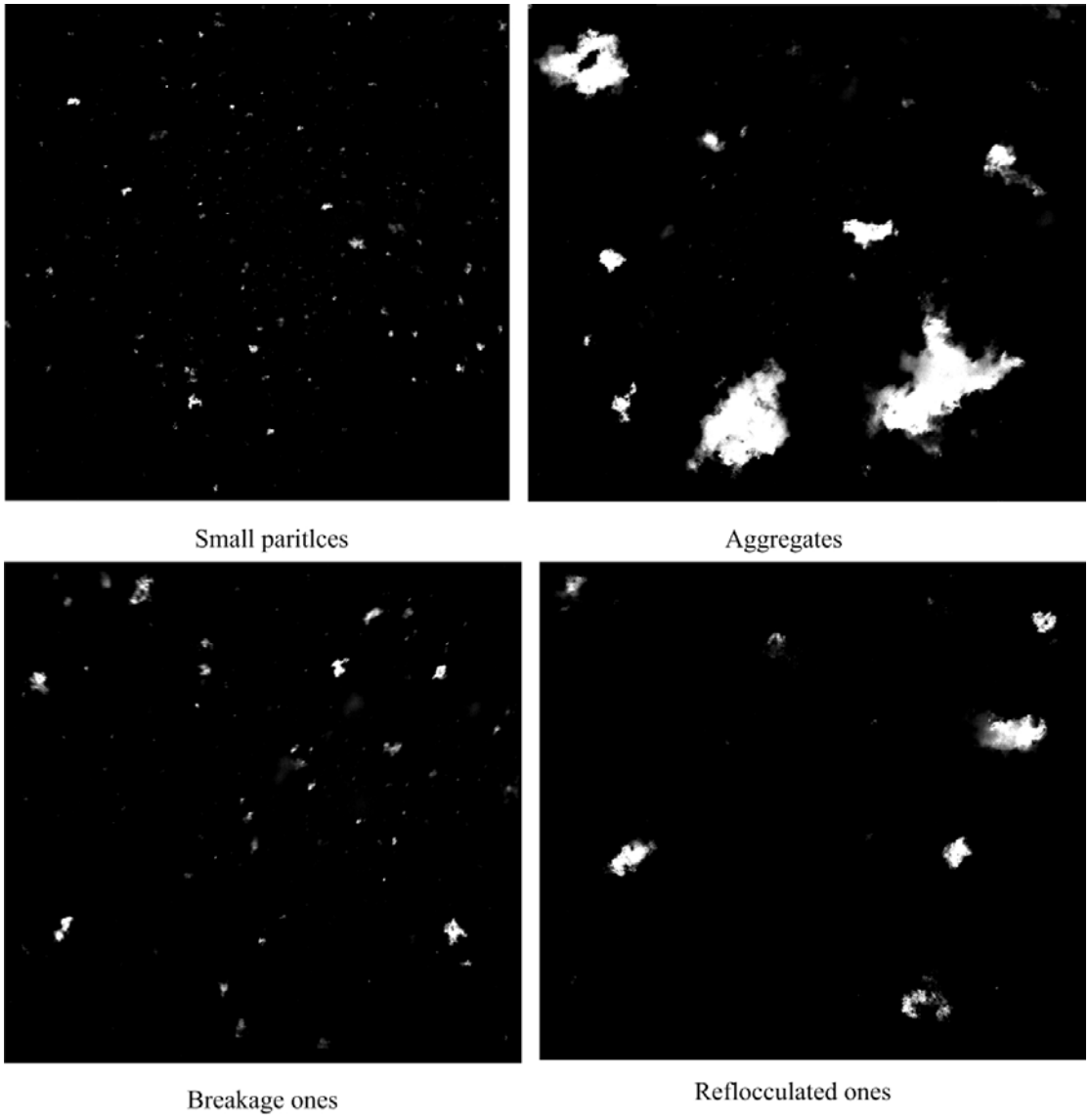

503
504

505 **Figure 6**. Examples of the PIV images of particle flocs during a typical A-B-R process.

506

507

508

509

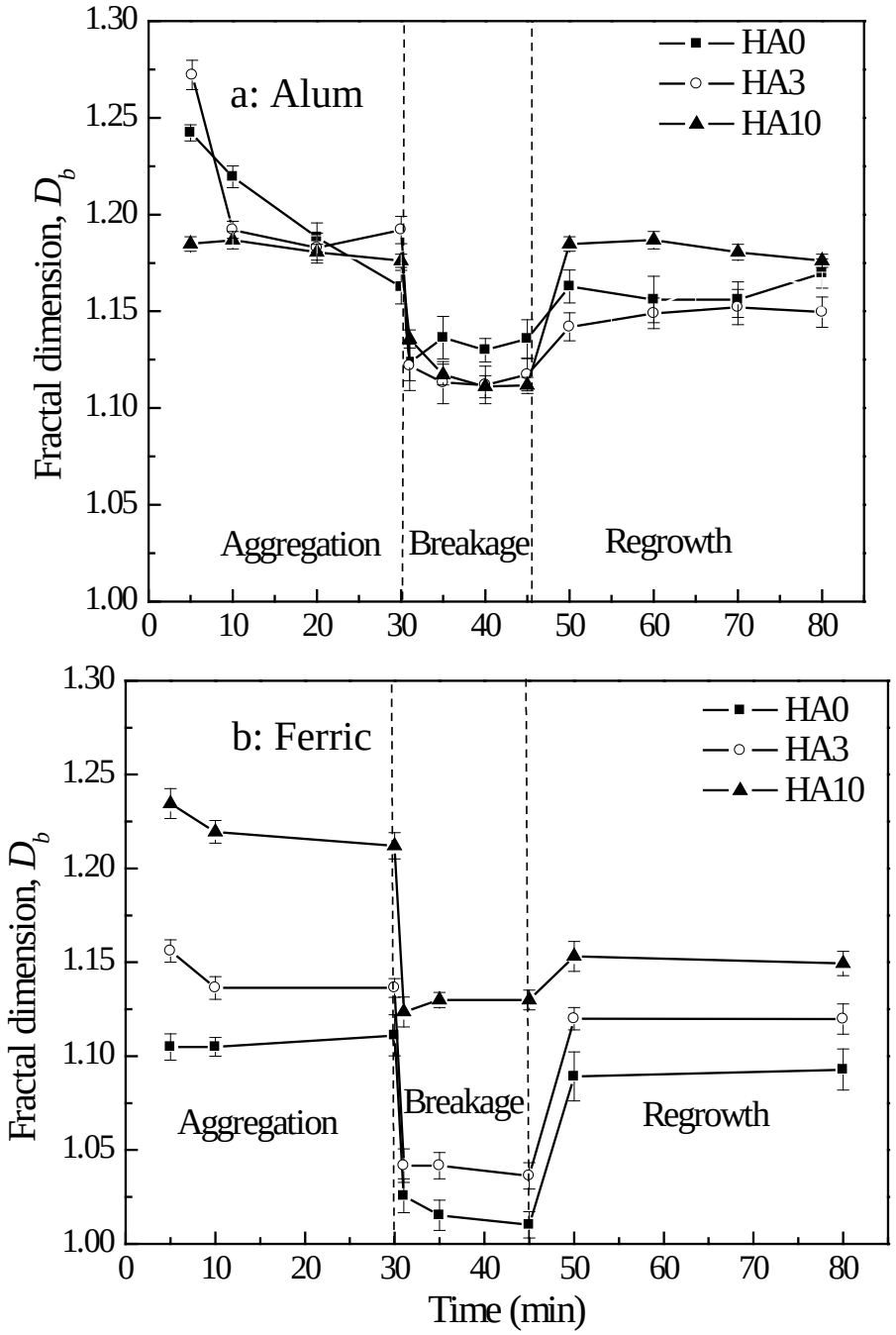

510

511 **Figure 7**. Change of the fractal dimension of the particle flocs with different HA contents in

512 water during the A-B-R tests.